Energetics Analysis of the Global Circulation during the Special Observation Periods of FGGE[1]

ERNEST C. KUNG AND HIROSHI TANAKA

Department of Atmospheric Science, University of Missouri-Columbia, Columbia, MO 65211

(Manuscript received 31 May 1983, in final form 21 July 1983)

ABSTRACT

A global energetics analysis is presented for the FGGE SOP-1 and SOP-2 with ECMWF and GFDL data sets. Both global integral properties and spectral characteristics are examined.

There is a large discrepancy between the present FGGE analysis and previously available estimates concerning the level of available potential energy and kinetic energy. This discrepancy is attributable to an earlier restriction of data coverage. There is a significant seasonal difference in the energy reservoir of the Northern Hemisphere, whereas the difference is minor in the Southern Hemisphere. This leads to a seasonal contrast of the globally integrated energy budget which comes mostly from the Northern Hemisphere. Both the global energy level and the intensity of the general circulation are more pronounced during SOP-1 than during SOP-2.

One major focus of attention in this study is an energetics comparison of ECMWF and GFDL data sets. There is a twofold difference in the intensity of the general circulation as measured with these two data sets. The energetics diagnosis indicates that the operational modes of the general circulation as described by these two data sets also differ considerably. The contrasts between SOP-1 and SOP-2 and between the ECMWF and GFDL versions of the data sets are apparent in the pattern of energy flow in the wavenumber domain.

1. Introduction

An energetics diagnosis with observed aerological data in the framework of primitive equations has long been hampered by inadequate coverage of the reporting upper air stations, restricting studies in this approach mostly to a diagnosis of ensemble energetics properties of limited spatial extent or case analysis of distinct synoptic systems. The availability of Level III data sets from the First GARP (Global Atmospheric Research Program) Global Experiment (FGGE) relieves the energetics study for the FGGE period from this difficulty. The four-dimensional assimilations of an unprecedented volume of meteorological data during this period—both conventional surface based data and new types of satellite data—provide adequate global grid coverage, making a comprehensive energetics diagnosis of global scale feasible. Yet, it is also expected that the global circulation models and techniques employed in data assimilation may exercise certain influences on the data sets produced.

In this study, the global energy budgets during the first and second special observation periods (SOP-1 and SOP-2) of FGGE are evaluated successively with two separate sets of FGGE Level IIIb data. The data were produced by the European Centre for Medium Range Weather Forecasts (ECMWF) with a slightly modified version of the operational assimilation system (Bengtsson *et al.*, 1982; Williamson and Temperton, 1981), and by the Geophysical Fluid Dynamics Laboratory (GFDL) with a FGGE data assimilation system (Miyakoda *et al.*, 1982). For reference purposes, limited use is also made of the Level IIIa data set, produced by the World Meteorological Center Washington with the National Meteorological Center (NMC) operational data assimilation system (McPherson *et al.*, 1979). These versions of FGGE data will be referred to hereafter as ECMWF, GFDL and NMC data sets, respectively. Through observational evaluation of FGGE energy budgets, we should add useful information to the existing knowledge of atmospheric energetics for a more comprehensive understanding of the global-scale circulation. An intercomparison of different versions of data sets in an energetics context may also make relevant references to FGGE research which involves these data sets.

Standard spectral and grid-point methods are utilized in computations of energetics in the zonal domain. Following a description of the data preparation and the analysis scheme, the evaluated energy budgets are presented in terms of global integrals, vertical profiles, meridional variations and spectral components. Gross energetics features of SOP-1 and SOP-2 are presented separately and contrasted to each other. In comparing energetics that are computed with different data sets, major attention is focused on the differences in the operational mode of the general circulation as described by ECMWF and GFDL data set versions. The effort

[1] Missouri Agricultural Experiment Station Contribution No. 9403.

is warranted because of the major FGGE task of observation, analysis and assimilation that went into producing these data sets and the expected usage of these data sets in the future.

2. Data preparation

The ECMWF, GFDL and NMC data sets for the periods 1 January–5 March 1979 and 30 April–7 July 1979 were obtained from the World Data Center A for Meteorology at Asheville, North Carolina. The ECMWF and GFDL data on a 1.87° × 1.87° latitude–longitude grid and the NMC data on a 2.5° × 2.5° grid were interpolated to the 4° × 5° grid with 46 latitudes from 90°S to 90°N and 72 longitudes from 0 to 355°E. The interpolation to each of the 4° × 5° grid points was done by a bilinear interpolation of four surrounding values of the original data sets at individual pressure levels. Adequacy of the interpolation was examined by comparing the fields of meteorological parameters in the original data and the interpolated data, and by interpolating back the obtained 4° × 5° grid values to the original smaller grids. Thirty randomly selected synoptic cases of interpolation–reinterpolation are visually examined to confirm that the patterns of the parameters remain unchanged.

The three data sets interpolated to the 4° × 5° grid include twice daily standard data of geopotential height, humidity, temperature and wind at 1000, 850, 700, 500, 400, 300, 250, 200, 150, 100, 70 and 50 mb at 0000 and 1200 GMT. The fields of vertical velocity ω are also available for ECMWF and GFDL versions from respective four-dimensional analyses of the FGGE observations. In the case of the NMC version, however, a kinematic field of ω was estimated with the interpolated field of wind at the 4° × 5° grid points with an assumption of $\omega = 0$ at the surface and a quadratic correction at the top of the atmosphere. The 4° × 5° grid data of individual observation times, thus prepared from the three data sets separately for the two data periods, constitute the basic input data for computational analysis.

3. Scheme of analysis

For the global energetics analysis, the computations in this study are based on standard methods of spectral energetics after Saltzman (1957, 1970) and energy variables that are directly computed at grid points.

The one-dimensional wavenumber equations of kinetic energy and available potential energy by Saltzman (1957, 1970) may be written as

$$\frac{\partial K_M}{\partial t} = \sum_{n=1}^{N} M(n) + C(P_M, K_M) - D(K_M), \quad (1)$$

$$\frac{\partial K(n)}{\partial t} = -M(n) + L(n) + C(n) - D(n),$$

$$n = 1, 2, 3, \cdots \quad (2)$$

$$\frac{\partial P_M}{\partial t} = -\sum_{n=1}^{N} R(n) - C(P_M, K_M) + G(P_M), \quad (3)$$

$$\frac{\partial P(n)}{\partial t} = R(n) + S(n) - C(n) + G(n),$$

$$n = 1, 2, 3, \cdots, \quad (4)$$

where all quantities represent integrals over the total mass of the atmosphere. The variables in Eqs. (1)–(4), listed in Table 1, follow definitions by Saltzman (1970). The equations of eddy kinetic energy and available potential energy may be obtained by summing Eqs. (2) and (4) from $n = 1$ to N where N is the maximum wavenumber:

$$\frac{\partial K_E}{\partial t} = -M(K_E, K_M) + C(P_E, K_E) - D(K_E), \quad (5)$$

$$\frac{\partial P_E}{\partial t} = R(P_M, P_E) - C(P_E, K_E) + G(P_E). \quad (6)$$

The kinetic energy equation averaged with respect to longitude may be written with pressure as the vertical coordinate:

$$\frac{\partial \bar{k}}{\partial t} = -\bar{\nabla} \cdot \overline{\mathbf{V}k} - \frac{\partial \overline{\omega k}}{\partial p} - \overline{\mathbf{V} \cdot \nabla \phi} - D, \quad (7)$$

where

$$k = \tfrac{1}{2}(u^2 + v^2). \quad (8)$$

The production term may be written as a summation of three process terms

$$-\overline{\mathbf{V} \cdot \nabla \phi} = -\overline{\nabla} \cdot \overline{\mathbf{V}\phi} - \frac{\partial \overline{\omega \phi}}{\partial p} - \overline{\omega \alpha}. \quad (9)$$

If Eqs. (7) and (9) are integrated with respect to latitude (i.e., for the global average), the first term of the right-hand side of the respective equation will vanish. Likewise, if Eqs. (7) and (9) are integrated with respect to latitude and pressure (i.e., over the entire mass of the atmosphere), the first two terms of the right-hand side of these equations will vanish. It is also noted here that the conversion term in Eq. (9) may be considered as a summation of conversion by mean meridional circulation and conversion by large-scale eddy convection, i.e.,

$$-\overline{\omega \alpha} = -\bar{\omega}''\bar{\alpha}'' - \overline{\omega' \alpha'}. \quad (10)$$

In Eqs. (1)–(7), dissipation terms of kinetic energy and generation terms of available potential energy are obtained as residual terms to balance the respective equations after other terms are evaluated with the data. For computation of spectral energetics, a program package obtained from the NASA Goddard Laboratory for Atmospheric Sciences (GLAS) was modified for use in this diagnosis. The GLAS program package is a refined version of the source program utilized by Baker *et al.* (1977, 1978) in diagnoses of the NCAR general circulation model. To compute available po-

TABLE 1. Symbols, definitions and variables.

p	pressure
t	time
u	eastward wind component
v	northward wind component
V	horizontal wind vector
k	kinetic energy per unit mass
m	mass of the atmosphere
α	specific volume
ω	vertical p-velocity $[=dp/dt]$
ϕ	geopotential
∇	horizontal del operator along an isobaric surface
$\bar{q}$	zonal average of an arbitrary function q
q'	departure of q from zonal average
$\bar{q}''$	departure of $\bar{q}$ from global average
n	zonal wavenumber
K	kinetic energy
K_M	zonal mean kinetic energy
K_E	zonal eddy kinetic energy
$K(n)$	K at wavenumber n
P	available potential energy
P_M	zonal mean available potential energy
P_E	zonal eddy available potential energy
$P(n)$	P at wavenumber n
$M(K_E, K_M)$	conversion from K_E to K_M
$M(n)$	conversion of $K(n)$ to K_M
$C(P_M, K_M)$	conversion from P_M to K_M
$C(P_E, K_E)$	conversion from P_E to K_E
$C(n)$	conversion of $P(n)$ to $K(n)$
$L(n)$	conversion of K_E from all other wavenumbers to $K(n)$
$R(P_M, P_E)$	conversion of P_M to P_E
$R(n)$	conversion of P_M to $P(n)$
$S(n)$	conversion of P_E from all other wavenumbers to $P(n)$
D	dissipation of k
$D(K_M)$	dissipation of K_M
$D(K_E)$	dissipation of K_E
$D(n)$	dissipation of $K(n)$
$G(P_M)$	generation of P_M
$G(P_E)$	generation of P_E
$G(n)$	generation of $P(n)$
$-\nabla \cdot V k$	horizontal flux convergence of kinetic energy
$-\partial \omega k/\partial p$	vertical flux convergence of kinetic energy
$-V \cdot \nabla \phi$	production of kinetic energy by cross-isobaric motion
$-\nabla \cdot V\phi$	horizontal flux convergence of potential energy
$-\partial \omega \phi/\partial p$	vertical flux convergence of potential energy
$-\omega\alpha$	baroclinic conversion from P to K
$-\omega'\alpha'$	baroclinic conversion by eddy convection
$-\bar{\omega}''\bar{\alpha}''$	baroclinic conversion by mean meridional circulation.

tential energy, the global mean static stability parameter is obtained at each level for each observation time. Values of the eddy variables are obtained as spectral sums over wavenumbers from $n = 1$ to 30. Values for the shorter wavenumbers do not contribute to spectral sums. The difference between the truncated energy value and the grid-point value by high-frequency noise is negligible. For the computation of variables involved in Eqs. (7) and (9), input data from the $4° \times 5°$ grid are used in direct computation at the individual grid points.

Energy budgets are computed for each observation time during the data periods. Averages of computed variables during the first data period are taken as values for SOP-1 and those during the second data period as values for SOP-2. The data periods used in this study are several days longer than the officially defined SOPs. For the convenience of the computational process and a general preference for longer data periods, no attempt was made to shorten the data periods. Energy variables in this paper are presented as integral values for the mass of the atmosphere between specified pressure levels as indicated by the physical units employed. The limits of integration for the vertical totals are from the surface to 50 mb.

4. Global energy balance

In examining the global energy balance, it will be beneficial to first evaluate the energy flow according to Lorenz's (1955) basic resolution of kinetic energy and available potential energy. In Fig. 1 the gross energy balances during SOP-1 and SOP-2 are presented as computed with both ECMWF and GFDL data set versions. In evaluating the energy balance in Fig. 1, $C(P_M, K_M)$ is obtained by

$$C(P_M, K_M) = -\int_m \mathbf{V} \cdot \nabla\phi dm - C(P_E, K_E), \quad (11)$$

utilizing the relationship stated in Eqs. (9) and (10). Substituting the indirectly obtained $C(P_M, K_M)$ for the directly computed value removes the dependence of $C(P_M, K_M)$ on the $\bar{\omega}$ field, which seems overly influenced by the data assimilation processes as will be discussed later. The values of $G(P_M)$ which would result from direct computation of $C(P_M, K_M)$ with the zonal mean field $\bar{\omega}$ are given in parentheses in Fig. 1 after the $G(P_M)$ values that are obtained with $C(P_M, K_M)$ by Eq. (11).

Despite considerable differences of computed energy balance between ECMWF and GFDL data sets and between SOP-1 and SOP-2, there is overall agreement on the direction of energy flow among them. Furthermore, the basic flow pattern agrees with previous observational estimates of the atmospheric energy cycle (e.g., Oort, 1964; Smagorinsky *et al.*, 1965; Manabe *et al.*, 1970; Newell *et al.*, 1970; Saltzman, 1970; Saltzman and Fleisher, 1960; Wiin-Nielsen, 1968). As shown in Fig. 1, the largest portion of energy transformation proceeds from P_M via P_E to K_E; whereas some K_E is further transformed to K_M. The dissipation takes place both in K_E and K_M. However, beyond this agreement, the numerical variations shown in the energy diagrams of Fig. 1 are considerable.

Average energy variables of SOP-1 and SOP-2 may be taken separately for ECMWF and GFDL data sets and compared in Table 2 with earlier observational estimates on an annual basis by Oort (1964), Oort and Peixoto (1974) and with that for the winter by Saltzman (1970). Although Oort and Peixoto's values are in the mixed space–time domain (see Oort, 1964) and some

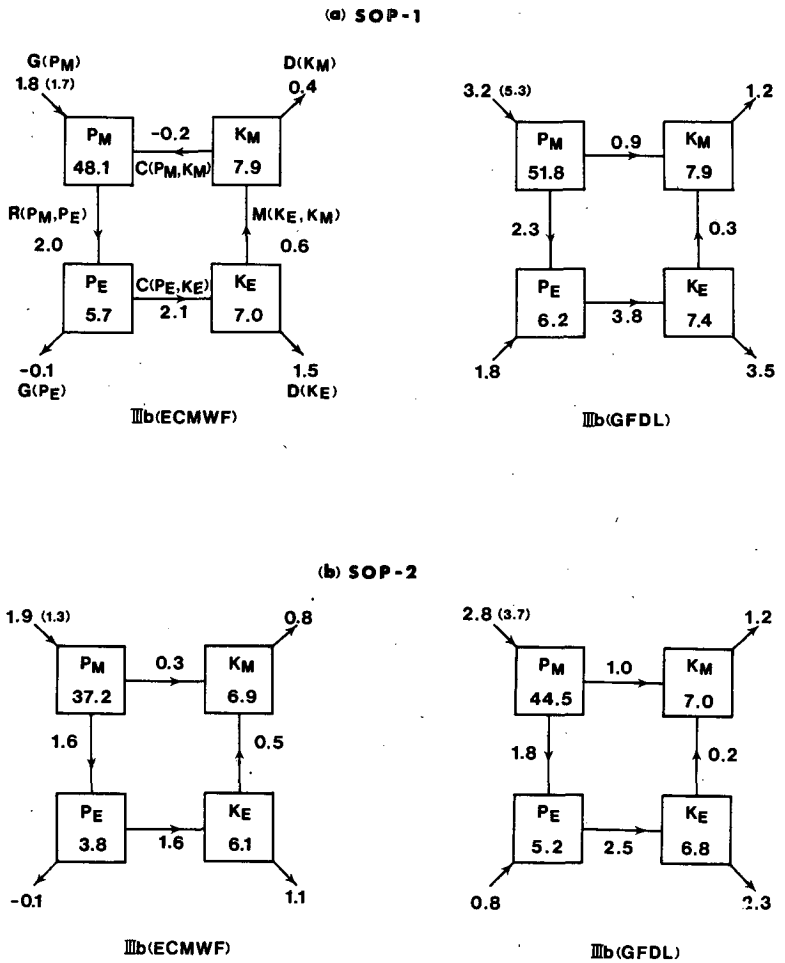

FIG. 1. Global energy balance during SOP-1 and SOP-2 with ECMWF and GFDL data sets. Energy is in units of 10^5 J m^{-2} and transformation in W m^{-2}.

discrepancy may be expected with regular analyses in the space domain, it may be readily noted that there is a large discrepancy between the present FGGE analysis and earlier estimates on the level of atmospheric energy. Both for the ECMWF and GFDL versions, the present analysis shows significantly larger P_M and

TABLE 2. Average energy variables of SOP-1 and SOP-2 with ECMWF and GFDL data sets compared with previous estimates by Oort (1964), Oort and Peixoto (1974) and Saltzman (1970). Energies are in units of 10^5 J m^{-2} and transformations in W m^{-2}.

Energy variables	SOP-1 and SOP-2 average		Annual mean after Oort (1964)	Annual mean after Oort and Peixoto (1974)	Winter mean after Saltzman (1970)
	ECMWF	GFDL			
P_M	42.7	48.2	40.0	33.5	35.5
P_E	4.8	5.7	15.0	15.6	11.3
K_M	7.4	7.5	8.0	3.6	10.0
K_E	6.6	7.1	7.0	8.8	14.3
$G(P_M)$	1.9	3.0	3.1	1.5	3.0
$G(P_E)$	−0.1	1.3	−0.8	0.7	−1.6
$R(P_M, P_E)$	1.8	2.1	3.0	1.5	5.3
$C(P_M, K_M)$	0.1	1.0	0.1	0.2	0.0
$C(P_E, K_E)$	1.9	3.1	2.2	2.2	3.0
$M(K_E, K_M)$	0.6	0.3	0.4	0.3	0.5
$D(K_M)$	0.6	1.2	0.5	0.1	0.5
$D(K_E)$	1.3	2.9	1.8	1.9	2.6
$D(K_M) + D(K_E)$	1.9	4.1	2.3	1.9	3.1

smaller P_E than previously estimated; in particular, the FGGE P_E is only ½ to ⅓ of the previously given P_E. The FGGE K_M and K_E are both around 7×10^5 J m^{-2} either by the ECMWF or the GFDL version, but it is difficult to compare them with earlier estimates as the latter vary greatly. As will be discussed later (see Figs. 2–5), spectral components of available potential energy and kinetic energy have characteristic latitudinal–seasonal distributions through the Northern and Southern Hemispheres. The earlier estimates were based on the observational network of the Northern Hemisphere; the coverages of the upper air stations were also much more sparse than in recent years and more restricted to the land areas of the middle latitudes. Thus, the energy levels and transformations of previous estimates are representative of the Northern Hemisphere middle latitudes whereas the values of the present study represent the global mean situation.

In comparing energy budgets computed with the ECMWF and GFDL data sets, however, the situation is clearly different. Both data set versions are global grid data for the same periods which have been produced from comparable original observations. In this study both data sets have been subjected to identical data preparation and computational analyses. Thus, the noticeable differences between the computed energetics should be directly attributed to the difference in the four-dimensional data assimilation processes involved in producing these data sets. Figs. 2–5 illustrate latitudinal distribution of available potential energy and kinetic energy in the wavenumber domain from $n = 0$ to 6 during SOP-1 and SOP-2. Energy levels computed with three data sets are plotted separately, and filled dots indicate coincided values of all three data sets. As shown in these figures, all three data sets, including the NMC version, yield similar spectral energy levels $P(n)$ and $K(n)$ except in the Antarctic region of the Southern Hemisphere. The difference of available potential energy among data sets (Figs. 2 and 3) is mainly due to the difference in $P(0)$ (i.e., P_M) and $P(1)$ in the Antarctic region, where observations are extremely sparse and data interpolation is heavily dependent on the models and techniques employed. Since the contribution of the Antarctic latitudes to global kinetic energy is limited (Figs. 4 and 5), the difference of the data sets in K_M and K_E is minor.

The intensity of the general circulation may be measured by the generation of available potential energy, the conversion of available potential energy to kinetic energy or the dissipation of kinetic energy. For the length of periods in this study we may expect

$$G(P_M) + G(P_E) = C(P_M, K_M) + C(P_E, K_E) = D(K_M) + D(K_E). \quad (12)$$

Since the terms $G(P_M)$, $G(P_E)$, $D(K_M)$ and $D(K_E)$ are obtained as residual terms of the respective energy equations, and the summation of $G(P_M)$ and $G(P_E)$ and that of $D(K_M)$ and $D(K_E)$ are dependent on the summation of $C(P_M, K_M)$ and $C(P_E, K_E)$, the intensity of the general circulation is explicitly determined by $-\mathbf{V} \cdot \nabla\phi$ in terms of total conversion through the relationship expressed in Eq. (11). The intensity measured with GFDL data sets is 4.1 W m^{-2} and that with the ECMWF data set is 1.9 W m^{-2} (Fig. 1 and Table 2). The former is approximately twice the latter, and this large difference is significant in view of its consistency through SOP-1 and SOP-2 and the compatibility of the two data sets in the source observations.

The twofold difference in the intensity of the energy cycle as shown with the ECMWF and GFDL data versions implies some fundamental differences in these data sets and thus in their description of the general circulation. For example, as compared in Figs. 6 and 7, the latitude–height cross sections of $\bar{\omega}$ indicate that, for both SOP-1 and SOP-2, the pattern of the mean meridional circulation is quite different as obtained with ECMWF or GFDL data sets, both for the position of mean meridional cells and their strength. Vertical profiles of the globally integrated $-\bar{\omega}''\bar{\alpha}''$ are shown in Fig. 8. Although this term is not used in evaluation of the energy balance and is substituted with an indirect estimate by Eq. (11), it is of interest to note the large contribution of this term in the GFDL version compared to the negligibly small contribution in the ECMWF version. The eddy conversion $-\omega'\alpha'$, with which $C(P_E, K_E)$ has been evaluated, shows in Fig. 9 that conversion of available potential energy to kinetic energy by synoptic-scale eddy convection is significantly more intense with the GFDL data than with the ECMWF data through most of the pressure layers. The baroclinic conversions computed with the NMC data set as shown by the vertical profiles in Figs. 8 and 9 indicate that the cell conversion $-\bar{\omega}''\bar{\alpha}''$ is essentially nonexistent and the eddy conversion $-\omega'\alpha'$ is the weakest among the three data sets.

Another important contrast of the ECMWF and GFDL data sets comes forth in observing the vertical profiles of the kinetic energy balance during SOP-1 and SOP-2 in Figs. 10 and 11. The well-recognized bimodal character of the kinetic energy production $-\mathbf{V} \cdot \nabla\phi$ and dissipation D (e.g., Kung, 1967, 1969, 1977; Smagorinsky *et al.*, 1965; Smith and Adhikary, 1974) is clearly observed with the GFDL data sets. During the past decade, a number of independent investigations on kinetic energy balance within the framework of primitive equations were conducted with aerological data which sampled regional phenomena of limited horizontal extent (e.g., Chen and Bosart, 1977; Fuelberg and Scoggins, 1980; Holopainen and Eerola, 1979; Kung and Chan, 1980). Those works collectively indicate that the cross-isobaric flow in the upper troposphere and the lower boundary provides the production mechanism by which the released available potential energy can appear as kinetic energy during the conversion process, and that the production

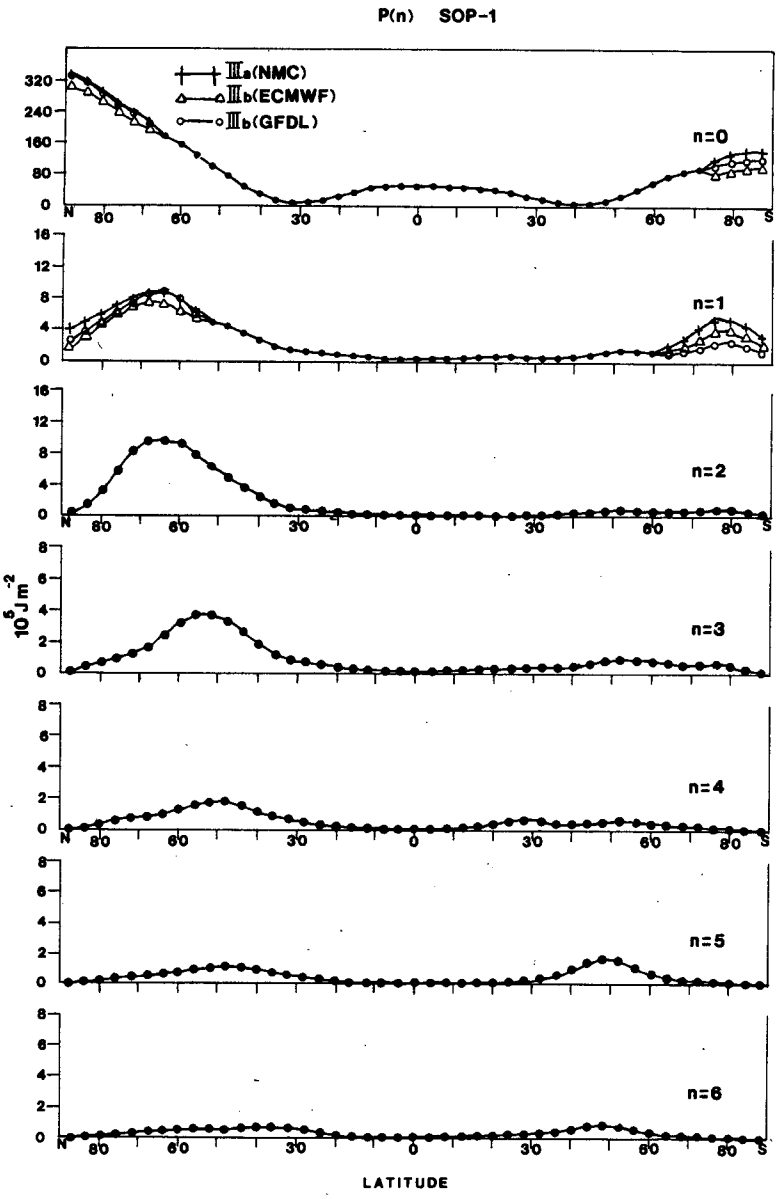

FIG. 2. Latitudinal distribution of available potential energy $P(n)$ from n = 0–6 during SOP-1 with ECMWF, GFDL and NMC data sets.

$-\overline{\mathbf{V}\cdot\nabla\phi}$ in its vertical distribution is roughly balanced by the dissipation D. Vertical profiles with GFDL data sets in this analysis seem to suggest that these are indeed characteristics of the global kinetic energy balance rather than simply regional phenomena. Vertical profiles of the kinetic energy balance by ECMWF data sets, however, show only a very small production and dissipation above the lower boundary. The less intense energy process given by the ECMWF version (Fig. 1 and Table 2) is thus associated with an obvious bias toward a geostrophic balance of the flow in the free atmosphere. This is a significant departure from the GFDL version which yields energetics features commonly observed in the framework of primitive equations.

The sharp contrasts in energy transformations that we observe with the ECMWF and GFDL versions are traced to the specific four-dimensional data assimilation processes involved in producing these data sets. For the ECMWF data set (Bengtsson *et al.*, 1982; Williamson and Temperton, 1981) the adiabatic nonlinear normal mode initialization of this version suppresses the divergent component of the wind. As shown in Figs. 6 and 7, vertical motion is generally underesti-

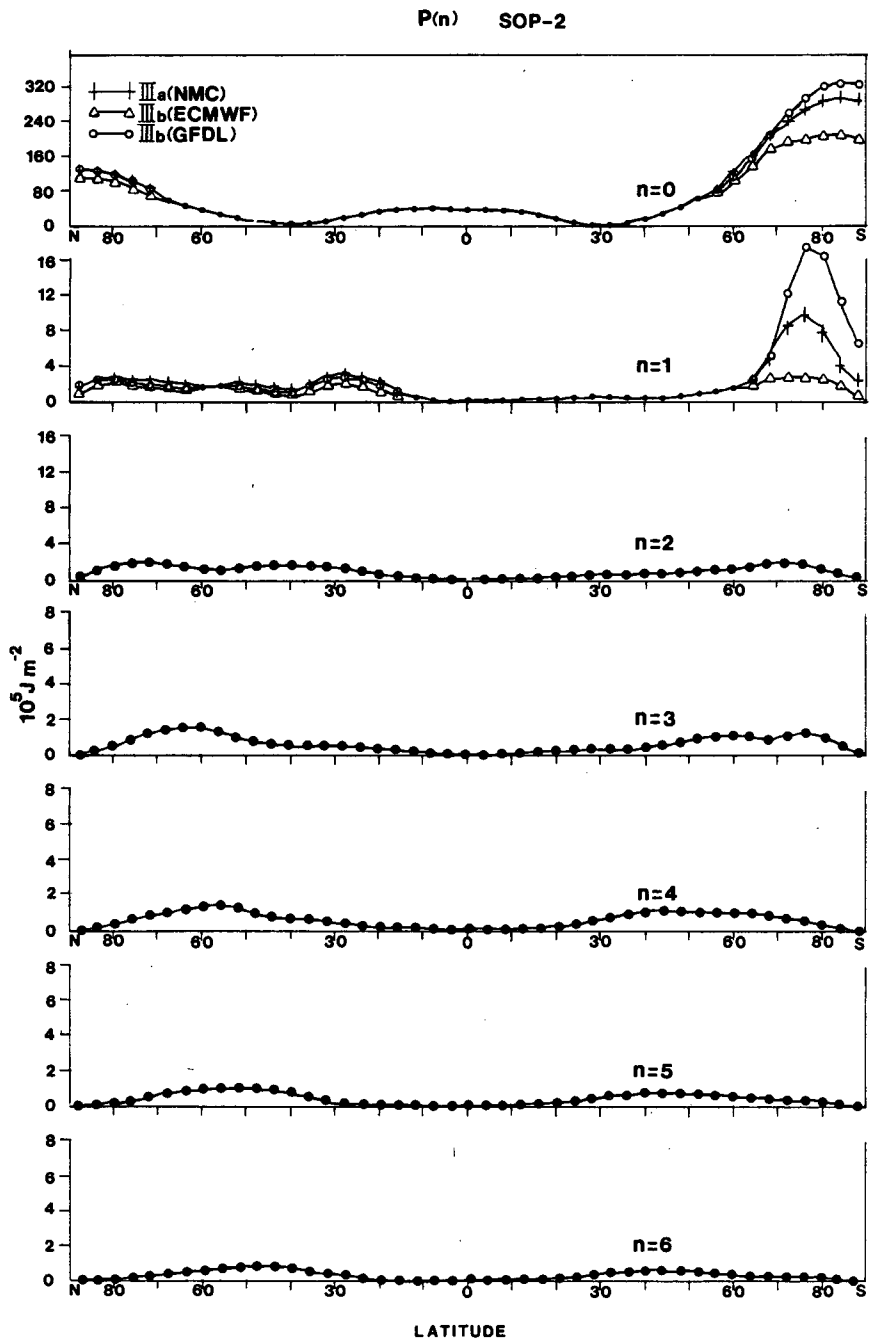

FIG. 3. As in Fig. 2, but for SOP-2.

mated and the underestimation is particularly severe in the Hadley cell region. Further, the assimilation of the ECMWF data set assumes a geostrophic-type relationship between height and wind in the middle and high latitudes. In assimilating the GFDL data set, the univariate optimum interpolation scheme utilized contains no geostrophic constraint. The normal mode adjustment between mass and wind fields for the GFDL version is made for only selected frequencies so that the basic characteristics of the atmospheric variables can be retained, including ageostrophic components, Hadley circulation, Kelvin and Rossby–gravity waves, etc. In view of the differences in the assimilation processes of these data sets, the revealed contrasts of energy transformations appear natural.

Since this is a global analysis, the contrasts between

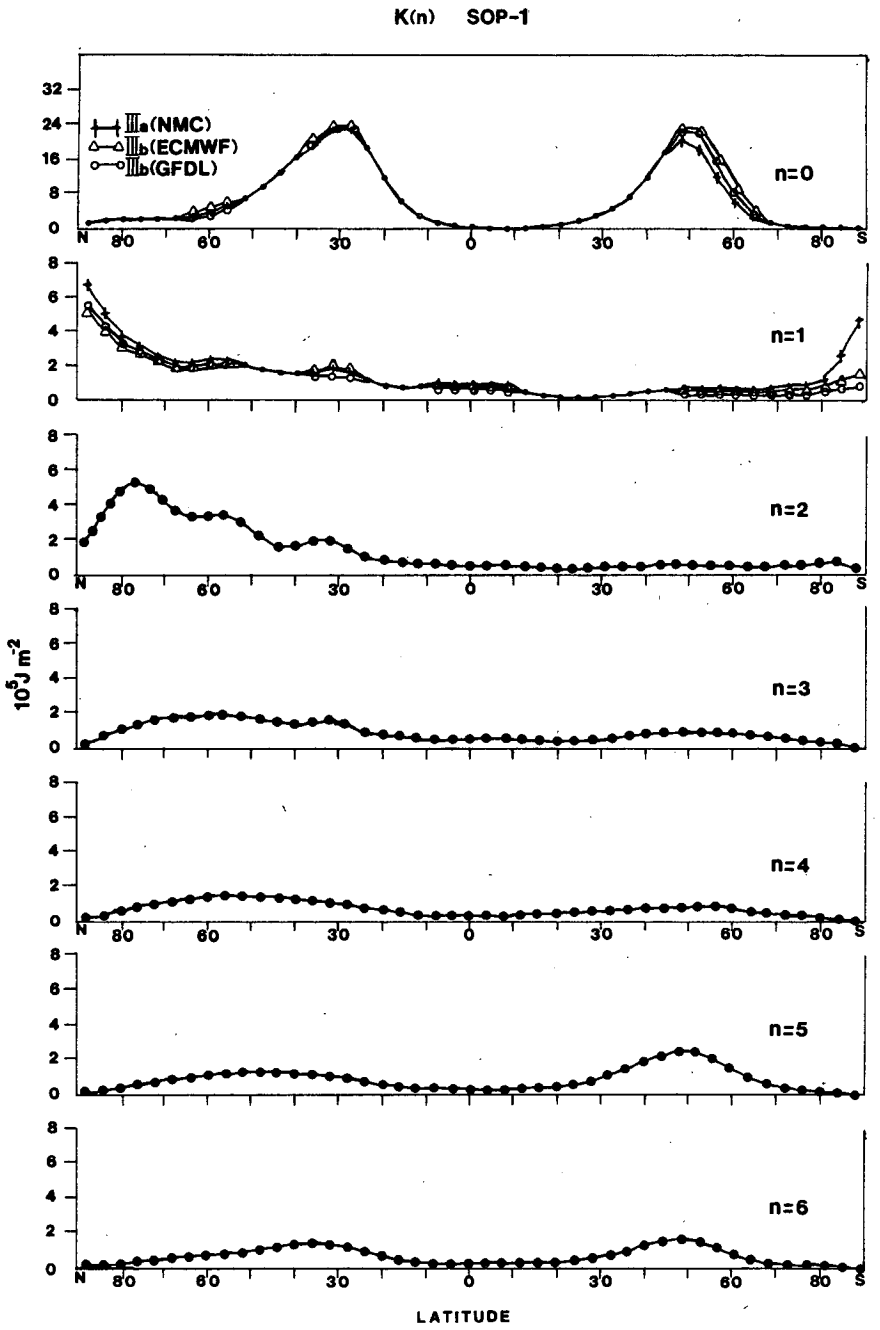

FIG. 4. Latitudinal distribution of kinetic energy $K(n)$ from $n = 0$–6 during SOP-1 with ECMWF, GFDL and NMC data sets.

SOP-1 and SOP-2 are interesting in that they reflect seasonal differences due to global latitudinal variations of the geophysical environment. The differences of energy levels between SOP-1 and SOP-2 shown in Fig. 1 are readily traced in spectral components in Figs. 2–5. In the middle to high latitudes of the Northern Hemisphere during SOP-1, $P(0)$ to $P(3)$ possess a high level of available potential energy, but during SOP-2, the levels diminish. In the Southern Hemisphere, the high latitudes show a higher energy level during SOP-2 than during SOP-1 only for $P(0)$ and $P(1)$; the contributions from other wavenumbers are not significant. In examining the latitudinal distribution of kinetic energy we see that during SOP-1 both hemispheres possess

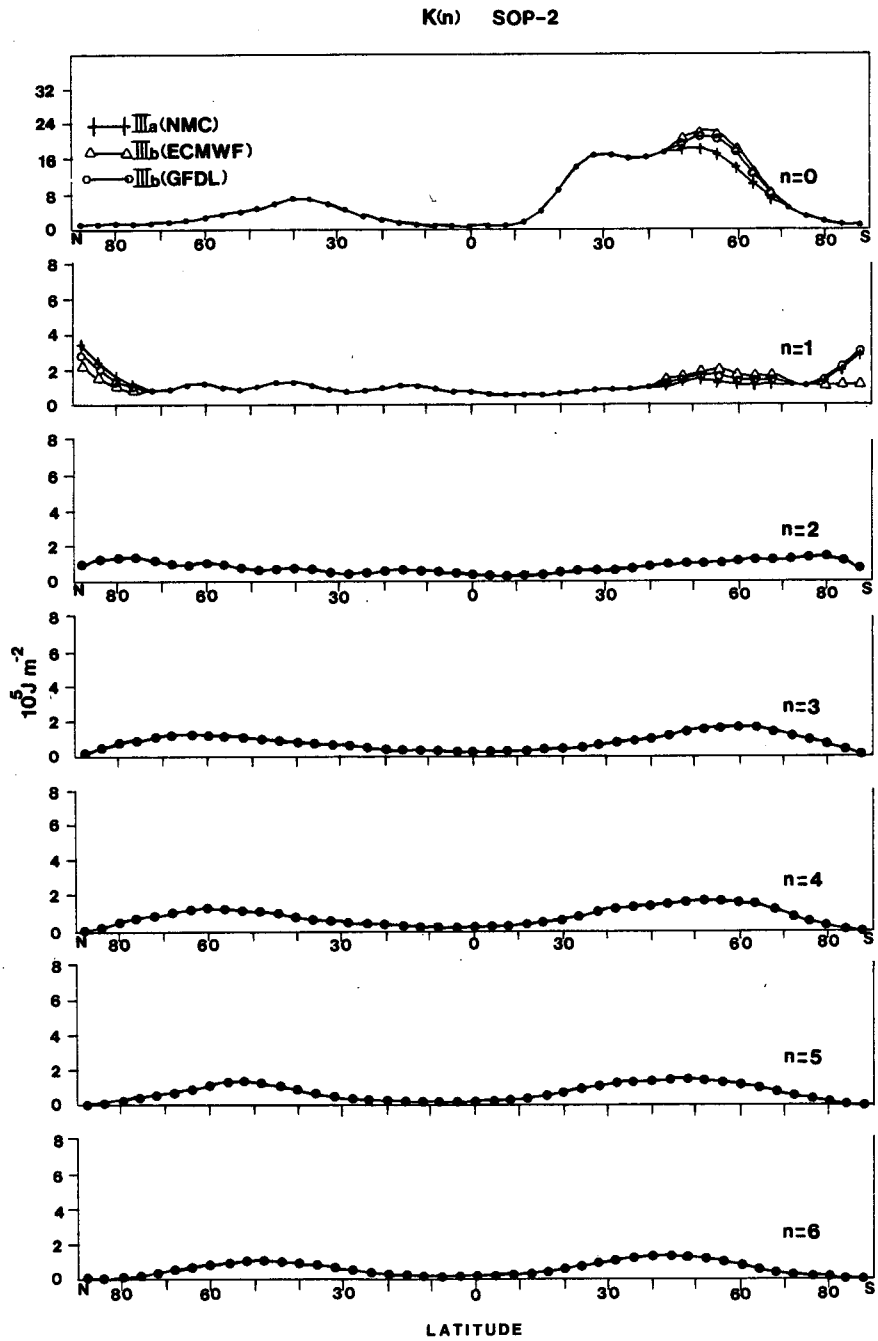

FIG. 5. As in Fig. 4, but for SOP-2.

high levels of $K(0)$ and the Northern Hemisphere further contributes significantly to K_E in the first two wavenumbers $n = 1$ and 2. During SOP-2, however, $K(0)$ is significant only in the Southern Hemisphere and this is the sole significant concentration of kinetic energy during SOP-2. The contribution to K_E at most wavenumbers in all latitudes during SOP-2 is not as outstanding as those of long waves in the Northern Hemisphere during SOP-1. These characteristic latitudinal–seasonal variations of energy components have resulted in generally higher global integrals of available potential energy and kinetic energy during SOP-1 than during SOP-2. The generally high levels of available potential energy and kinetic energy during SOP-1 are reflected by the more intense energy cycle (Fig. 1) and more pronounced vertical profile of production

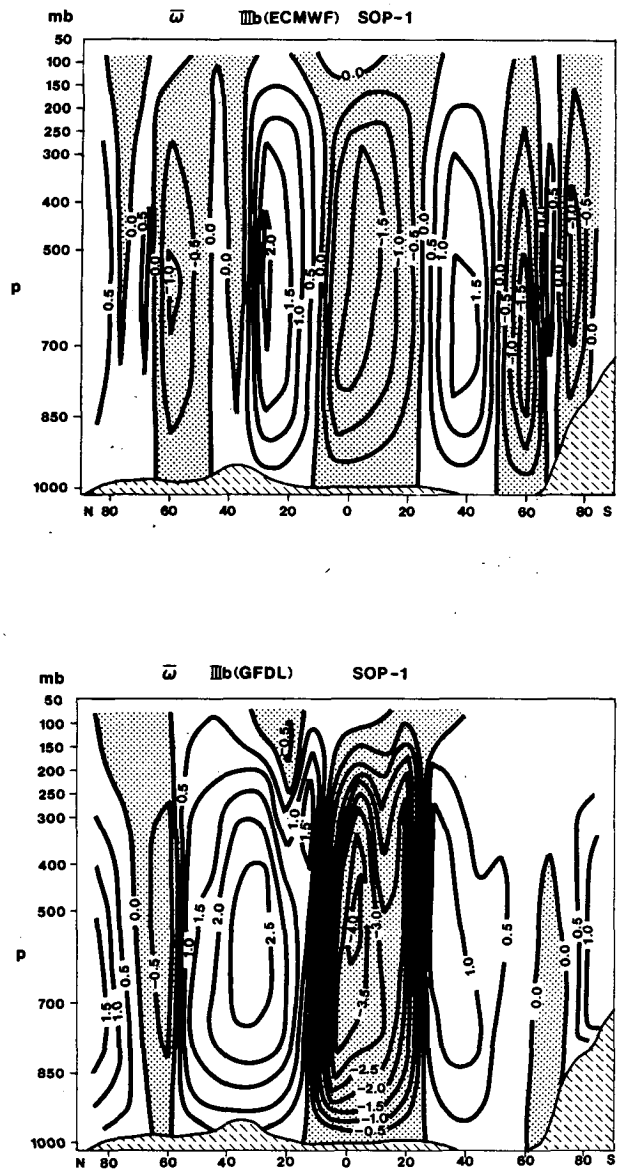

FIG. 6. Latitude-height distribution of $\bar{\omega}$ during SOP-1 with ECMWF and GFDL data sets; $\bar{\omega}$ in units of 10^{-1} μb s^{-1}.

$-\overline{\mathbf{V}\cdot\nabla\phi}$ and dissipation D (Figs. 10 and 11) during this period than during SOP-2. In association with kinetic energy production, the baroclinic conversions by the eddies $-\omega'\alpha'$ and by the mean meridional motions $-\bar{\omega}''\bar{\alpha}''$ are also significantly greater during SOP-1 than during SOP-2 (Figs. 8 and 9).

The two special observation periods, as covered in this study, do not represent exactly two observation periods half a year apart. Still, it is useful to take their average energy variables as an approximation to the mean global energy budget, which is done separately for the ECMWF and GFDL data sets in Table 2. Table 3 lists the vertical distribution of kinetic energy transformations with the GFDL data set averaged for SOP-1 and SOP-2 in the specified layers. These global integral quantities over a reasonably long period shall numerically approximate the global profiles of kinetic energy balance. As shown in Table 3, the dissipation in the 400–50, 700–400 and surface–700 mb layers are, respectively, 2.06, 0.41 and 1.66 W m^{-2} with a total of 4.13 W m^{-2}. It is noteworthy that the generation and dissipation in the 400–50 mb layer seems larger than, or at least in a similar magnitude as, in the surface–700 mb layer in this global budget. As indicated by model experiments (e.g., Smagorinsky *et al.*, 1965) and also implicitly recognized by earlier investigators (see Oort, 1964; Saltzman, 1970), the vertical distribution of $-\omega'\alpha'$ in Table 3 shows that the

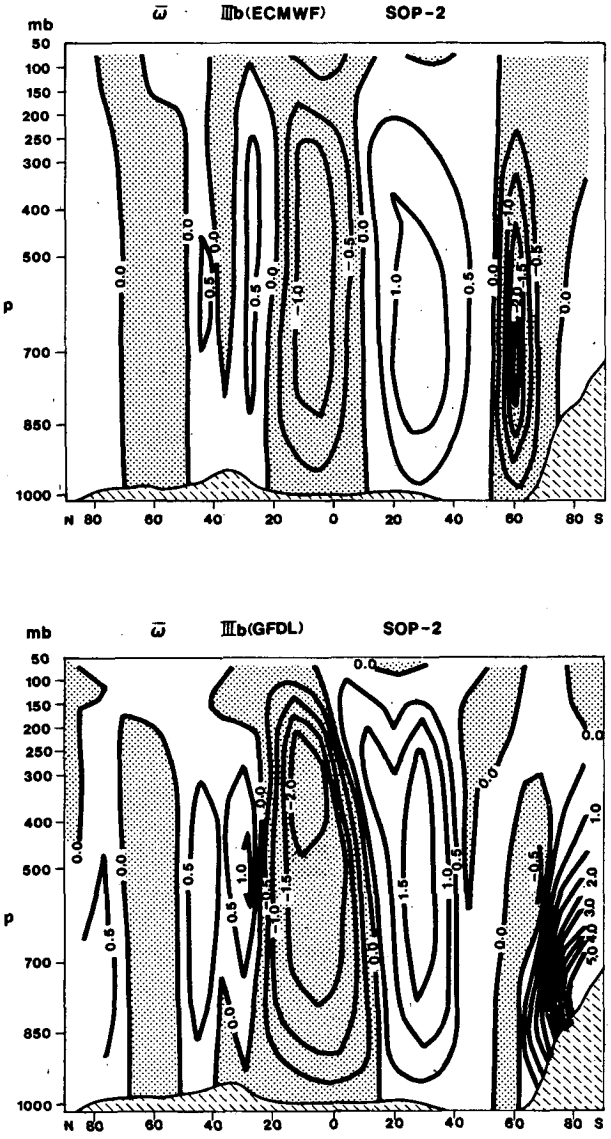

FIG. 7. As in Fig. 6, but for SOP-2.

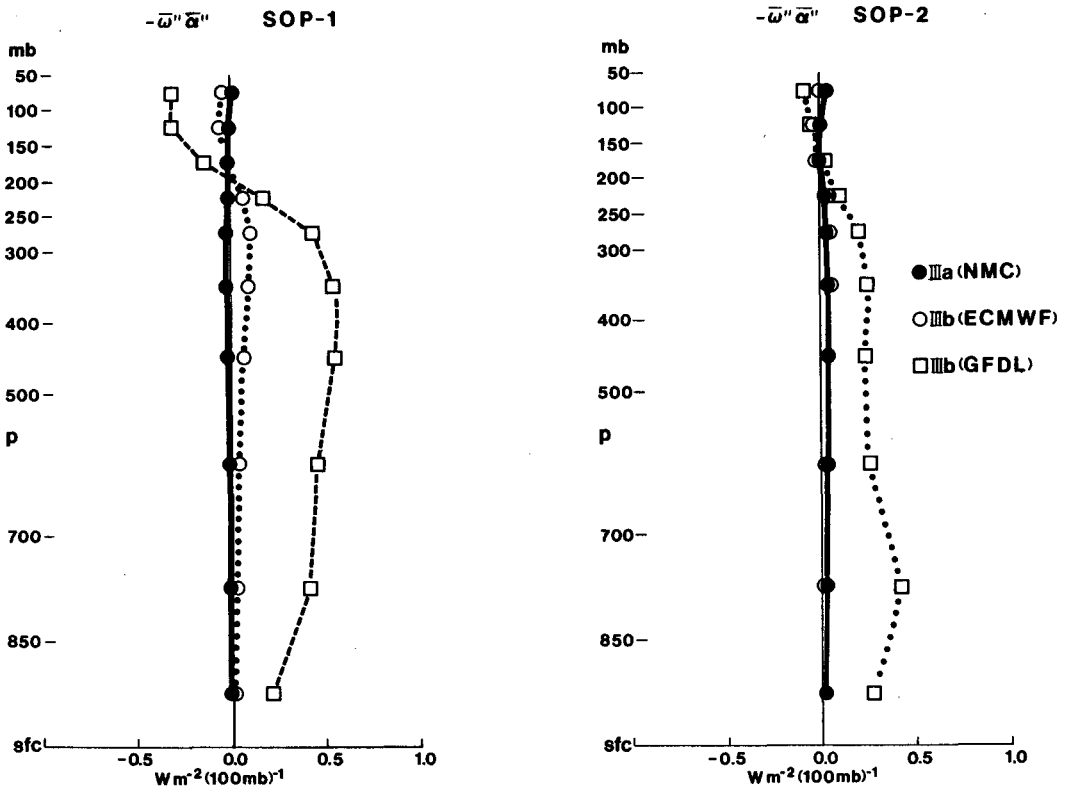

FIG. 8. Vertical profile of the global energy conversion $-\bar{\omega}''\bar{\alpha}''$ by the mean meridional circulation during SOP-1 and SOP-2 with ECMWF, GFDL and NMC data sets.

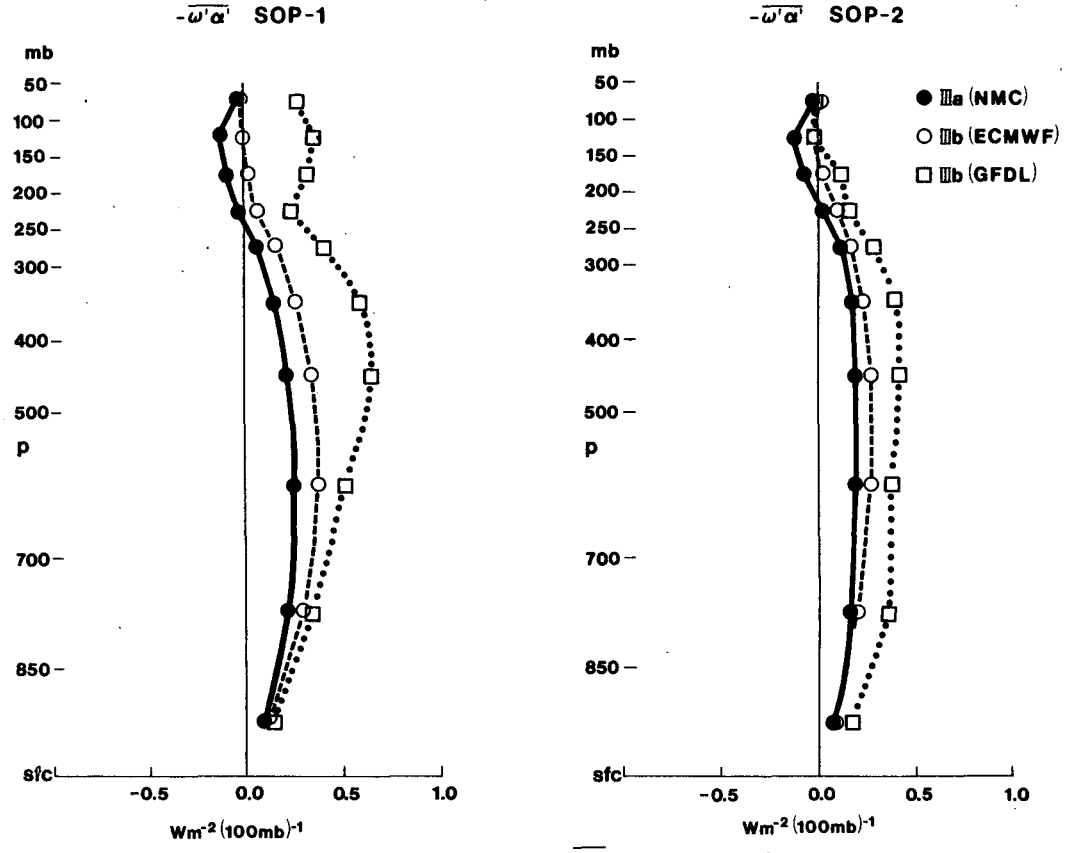

FIG. 9. As in Fig. 8, but for $-\overline{\omega'\alpha'}$ by the zonal eddies.

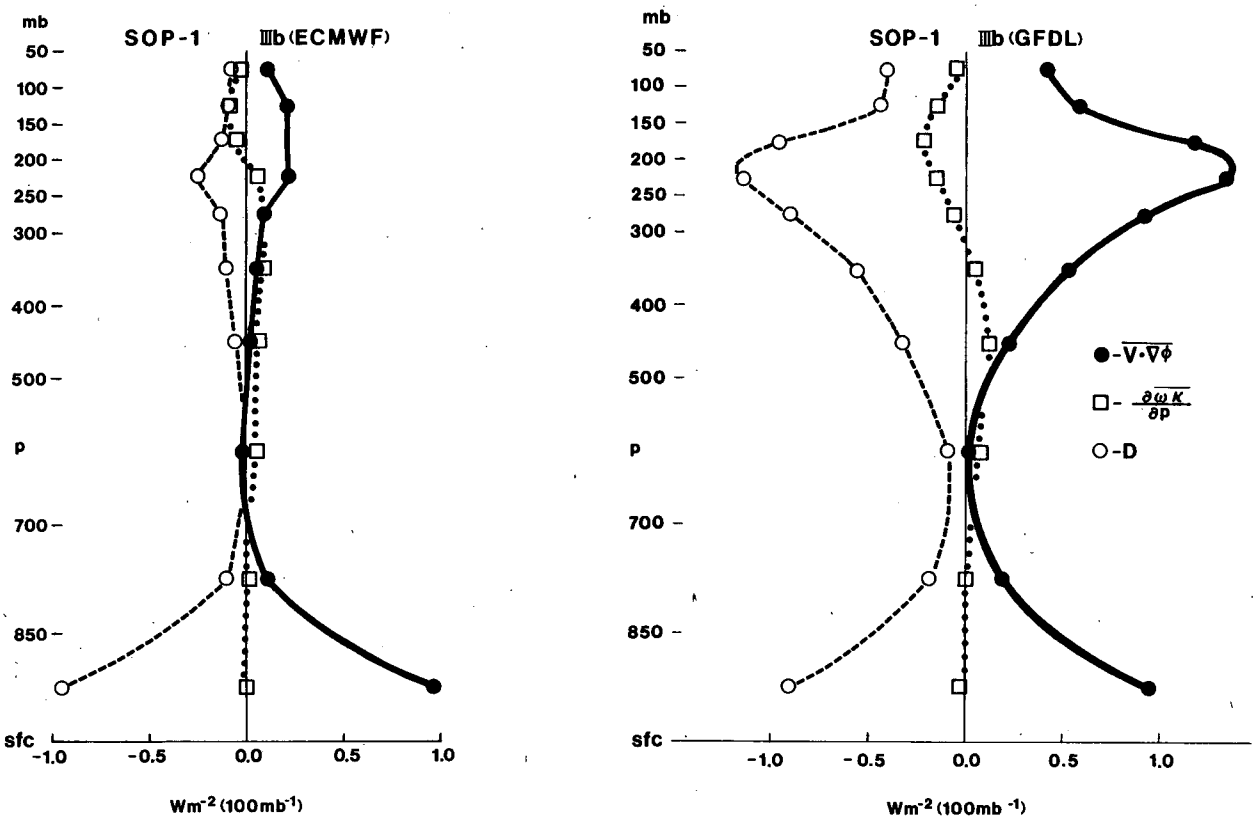

FIG. 10. Vertical profile of the global kinetic energy balance during SOP-1 with ECMWF and GFDL data sets.

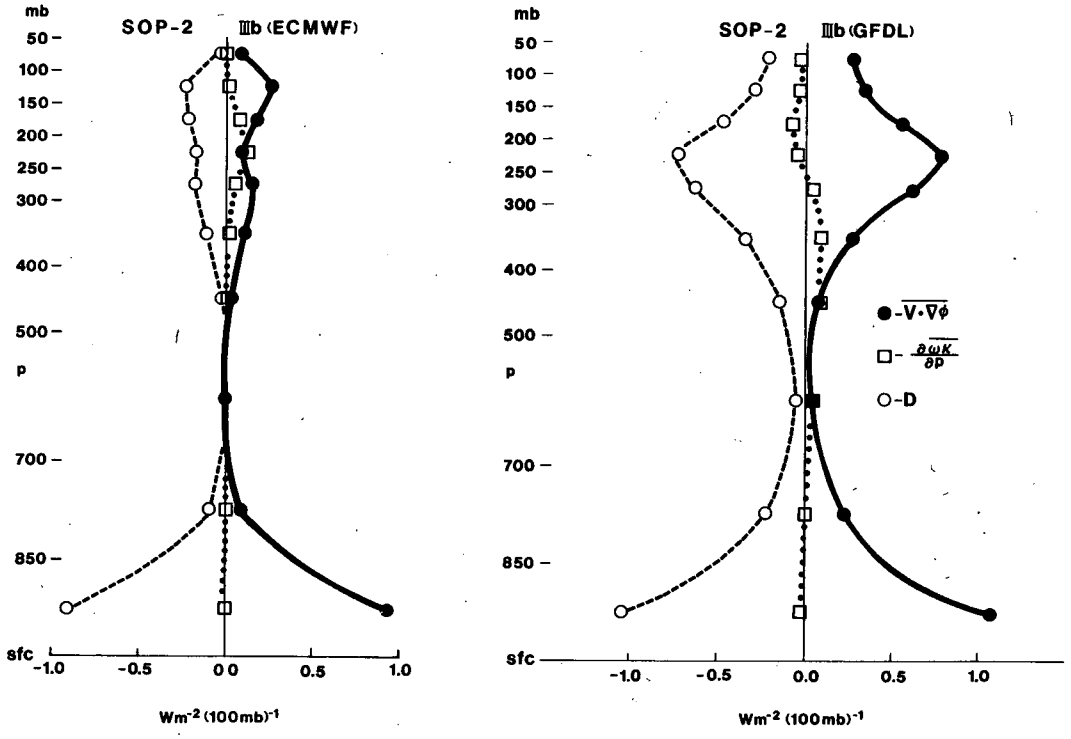

FIG. 11. As in Fig. 10, but for SOP-2.

TABLE 3. Averaged global energy transformations with GFDL data set for SOP-1 and SOP-2 for specified layers in units of W m^{-2}.

Pressure layer (mb)	$-\overline{\mathbf{V}\cdot\nabla\phi}$	$-\overline{\frac{\partial\omega k}{\partial p}}$	D	$-\overline{\omega'\alpha'}$
100–50	0.18	−0.01	0.16	0.06
150–100	0.23	−0.04	0.19	0.08
200–150	0.44	−0.07	0.37	0.11
250–200	0.53	−0.05	0.48	0.09
300–250	0.39	0.01	0.39	0.17
400–300	0.40	0.06	0.46	0.51
500–400	0.15	0.10	0.25	0.53
700–500	0.07	0.10	0.16	0.86
850–700	0.30	0.00	0.30	0.52
SFC–850	1.38	−0.03	1.35	0.21
400–50	2.17	−0.11	2.06	1.03
700–400	0.22	0.20	0.41	1.39
SFC–700	1.68	−0.03	1.66	0.72
Total	4.08	0.06	4.13	3.14

eddy conversion actively takes place in most of the troposphere with its maximum at the mid troposphere. The vertical total of $-\overline{\omega'\alpha'}$ is 3.14 W m^{-2}, and is 77% of the production $-\overline{\mathbf{V}\cdot\nabla\phi}$, indicating that approximately ¾ of the kinetic energy drawn from the reservoir of available potential energy is by the zonal eddies and the remaining ¼ by the mean meridional circulation.

5. Energy transformations in the wavenumber domain

Spectral characteristics of the global energy budgets during SOP-1 and SOP-2 are presented separately for the ECMWF and GFDL data sets from n = 0–15 in energy diagrams in Figs. 12–15. The energy diagram format follows that of Saltzman (1970) with the energy level and wavenumber in each box and the amount of energy flow between different energy components accompanied by an arrow sign for direction. The values for $G(0)$, $C(0)$ and $D(0)$ are as listed in Fig. 1 for the zonal means of available potential energy and kinetic energy, whose evaluation involves both spectral energy and grid variable computations as described in the preceding section. In presenting the results, no specific attempt has been made to adjust computational errors in order to balance the wave interactions.

As has been discussed, there is close agreement of energy levels as computed with ECMWF and GFDL data sets, but there is a significant difference between the present FGGE results and the previous observational studies (see Fig. 1 and Table 2). In observing the spectral distribution of $P(n)$ and $K(n)$, we again see good agreement between the ECMWF and GFDL versions. In comparing the present FGGE analysis with Saltzman's (1970) winter estimate, the differences are in the long and mid-range waves. For $P(n)$ from n = 1–7, Saltzman's diagram lists 30, 24, 15, 11, 8, 6 and 5×10^4 J m^{-2}, respectively, and for $K(n)$ from n = 1–9, it is 24, 19, 20, 16, 14, 11, 8, 9 and 7×10^4 J m^{-2}. The significantly lower energy level in this wave range in the present global analysis, as shown in Figs. 12–15, is apparently due to the inclusion of the tropics and the Southern Hemisphere, where energy in this wave range is less (Figs. 2–5). Contrasts of $K(n)$ and $P(n)$ between the Northern and Southern Hemispheres in these specific wavenumber ranges should be attributable to the difference in both hemispheres of land–sea distribution and topography.

As discussed in the preceding section, the intensity of the general circulation measured with the GFDL data set is about twice that measured with the ECMWF data set (Fig. 1 and Table 2). Comparing the transformations of these two versions in the wavenumber domain, it is seen in Figs. 12–15 that the conversion $C(n)$ and dissipation $D(n)$ are stronger at all wavenumbers with the GFDL version, and that their values are still significant at the shorter wave range. It is particularly interesting to note that, from n = 11–15, $D(n)$ is noticeably larger with the GFDL version, whereas it becomes negligible with the ECMWF version. Active conversion and dissipation in the shorter wave range is consistent with Saltzman's (1970) estimate. The negligibly small values of the ECMWF version in this range indicate that the energetically active synoptic-scale processes at this range are dampened. With the GFDL version, the eddy components of $G(n)$ are consistently positive, but with the ECMWF version, it fluctuates between small positive and small negative values with a zero value in the shorter wave range. There is a better agreement between the ECMWF and GFDL versions for the spectral distribution of $R(n)$ and $M(n)$ which describes the transformation between zonal and eddy components of energy. For $S(n)$ and $L(n)$, which describe the interactions among waves, however, the agreement between the two versions is marginal.

The contrast of SOP-1 and SOP-2 in energy transformation in the wavenumber domain is conspicuous in the energy diagrams of the GFDL version. During SOP-1, except for the very long waves, eddy generation of available potential energy, eddy conversion from available potential energy to kinetic energy and eddy dissipation are all more intense in all wavenumbers than during SOP-2 (Figs. 13 and 15). During SOP-1, the shorter waves from n = 11–15 are still very active with fairly large values of $G(n)$, $C(n)$ and $D(n)$, whereas during SOP-2, the intensity of transformations in this range is much weakened. With the ECMWF version (Figs. 12 and 14), higher levels of eddy conversion and dissipation during SOP-1 are also observed to a limited degree with long waves. From the prior discussion concerning the characteristically different seasonal variation in the energy reservoir of the Northern and Southern Hemispheres, it could be inferred that the more active eddy energy transformations during SOP-

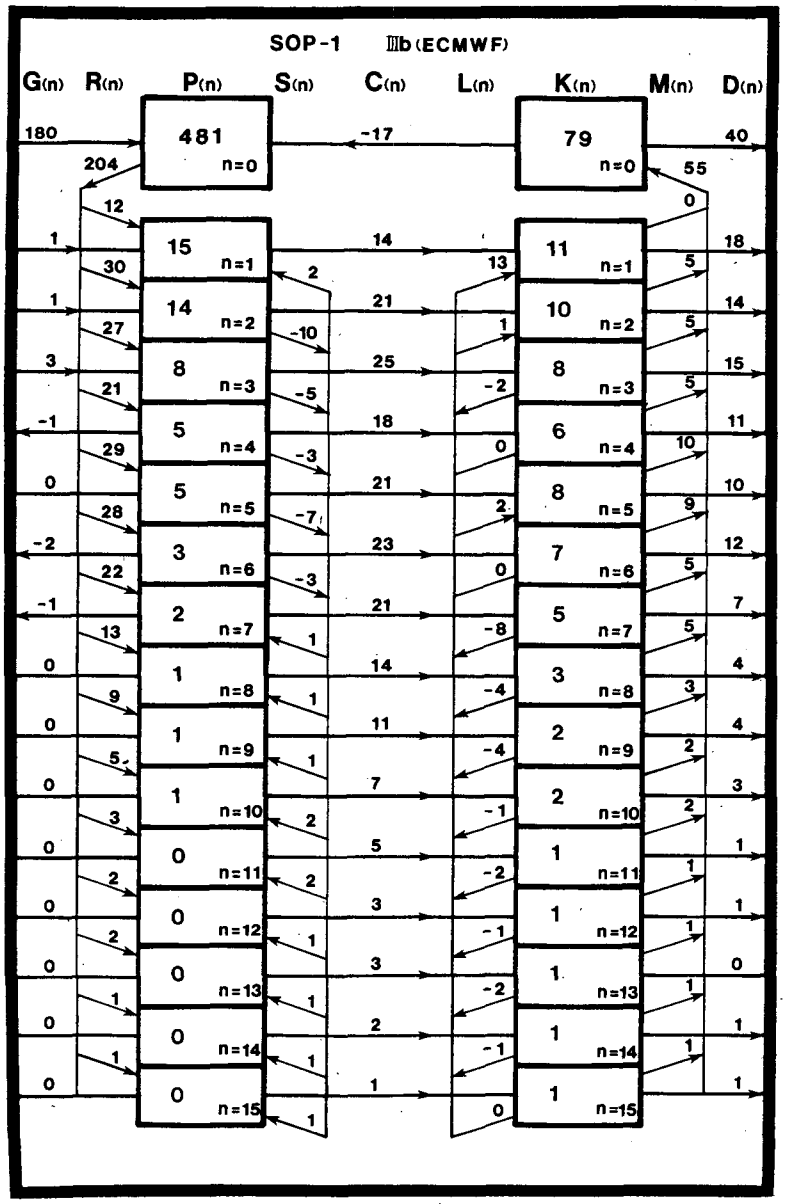

FIG. 12. Energy flow diagram in the wavenumber domain during SOP-1 with ECMWF data set. Energy is in units of 10^4 J m^{-2} and transformation in 10^{-2} W m^{-2}.

1 are tied to the contribution of synoptic disturbances in the Northern Hemisphere. Indeed, the computed values of eddy conversion $C(P_E, K_E)$ with the GFDL data for the Northern and Southern Hemispheres are 4.3 and 3.2 W m^{-2} for SOP-1 and 2.4 and 2.7 W m^{-2} for SOP-2.

6. Concluding remarks

Several points revealed in the present global energetics analysis may appear noteworthy. The present study notes an overall agreement with previous studies on the direction of energy flow in the wavenumber domain. However, there is a large discrepancy between the present FGGE analysis and previous estimates concerning the level of zonal mean and eddy components of available potential energy and kinetic energy, apparently due to the earlier restriction of data coverage. Seasonal variation in the reservoir of available potential energy and kinetic energy in the Northern Hemisphere is much greater than in the Southern Hemisphere. Consequently both the energy level and

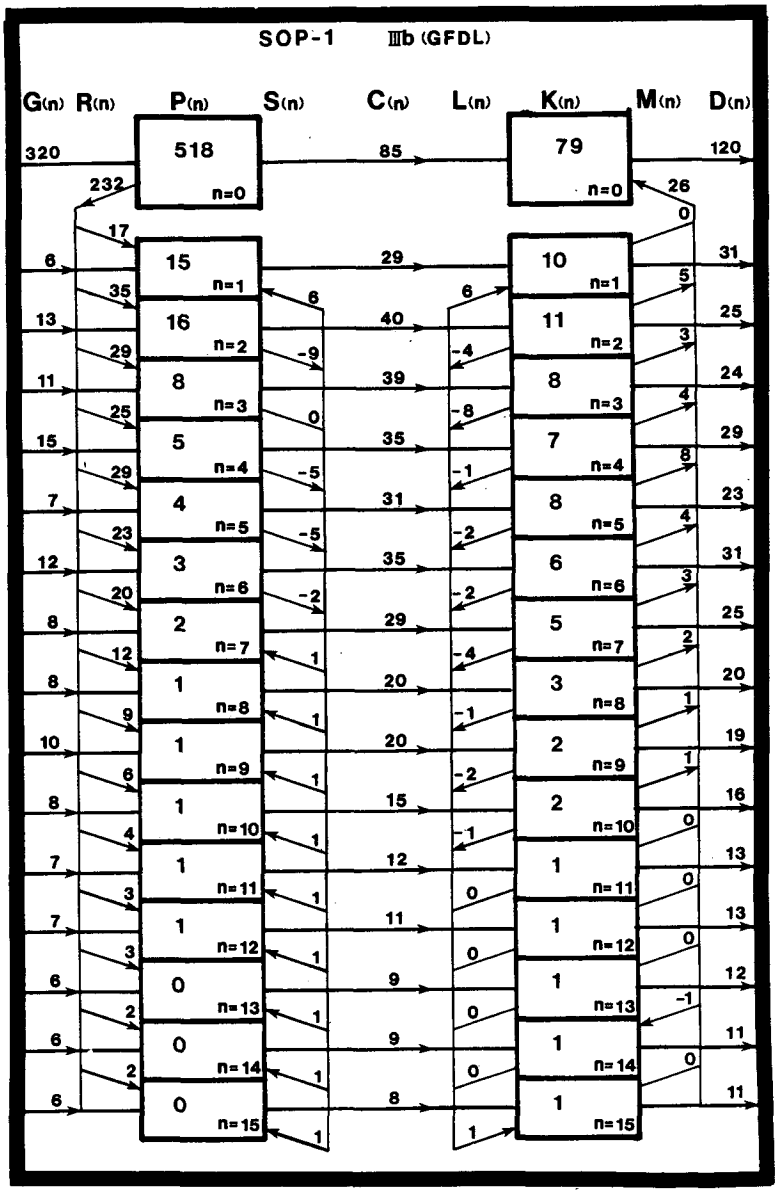

FIG. 13. As in Fig. 12, but for GFDL data set.

the intensity of the energy cycle are more pronounced during SOP-1 than during SOP-2.

There is a twofold difference in the intensity of the general circulation as measured with the ECMWF and GFDL data set versions. The difference is traced to the four-dimensional data assimilation processes of these data sets. The zonal mean field of vertical motion and vertical distributions of transformation variables indicate a substantial difference in the operational mode of the general circulation as described with these two FGGE Level IIIb data sets. The GFDL version shows energetics features commonly observed in the framework of primitive equations, but the ECMWF version leans toward a geostrophic balance of flow in the free atmosphere.

The often observed bimodal vertical profiles of kinetic energy production $-\overline{\mathbf{V}}\cdot\overline{\nabla\phi}$ and dissipation D with maxima in the upper troposphere and the lower boundary in the regional studies and the numerical experiment appear to be global integral characteristics. Approximately ¾ of the kinetic energy produced is through the process of eddy conversion $-\overline{\omega'\alpha'}$ with its

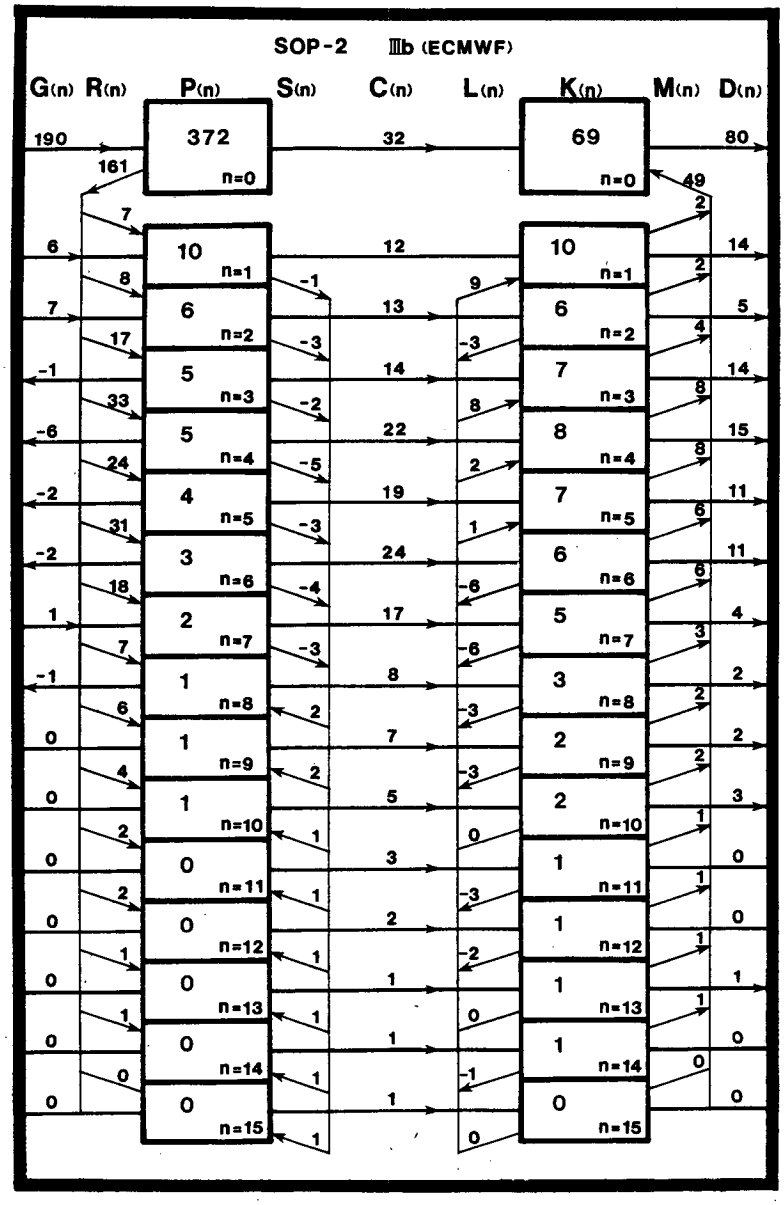

FIG. 14. Energy flow diagram in the wavenumber domain during SOP-2 with the ECMWF data set. Energy is in units of 10^4 J m^{-2} and transformation in 10^{-2} W m^{-2}.

maximum in the mid troposphere, the remaining ¼ is by meridional circulation.

Contrasts between the ECMWF and GFDL versions and between SOP-1 and SOP-2 are also apparent in the pattern of energy flow depicted in the wavenumber domain. The conversion $C(n)$ and dissipation $D(n)$ are stronger at all wavenumbers with the GFDL version. In the shorter wave range of n = 11–15 they are still significantly large with the GFDL version, whereas they become negligibly small with the ECMWF version. During SOP-1, $G(n)$, $C(n)$ and $D(n)$ are all more intense than during SOP-2 in most of the eddy wave range.

The present gross energetics analysis is intended to be a basic analysis of the FGGE SOPs. It indicates the usefulness of further studies of global and regional energetics with FGGE data sets. Recognizing specific characteristics of the FGGE data sets, such an endeavor shall be meaningful by enhancing our understanding of atmospheric processes in reference to maintenance and variations of the general circulation.

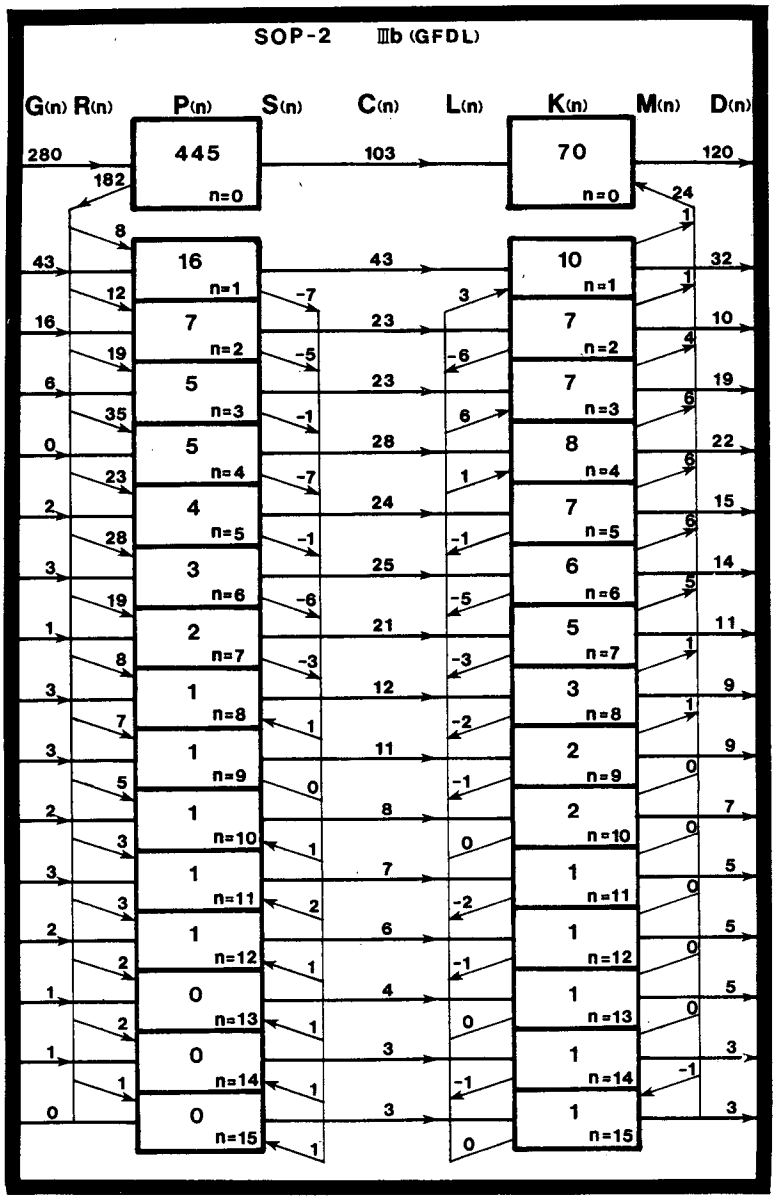

FIG. 15. As in Fig. 14, but for GFDL data set.

Acknowledgments. The authors sincerely appreciate the courteous arrangement by Dr. W. E. Baker of NASA Goddard Laboratory for Atmospheric Sciences in providing the basic spectral energetics code, and by Mr. R. L. Williams of NOAA Environmental Data and Information Service for the data supply. They are thankful to Dr. K. Miyakoda and Dr. A. H. Oort of NOAA Geophysical Fluid Dynamics Laboratory/Princeton University for their consultation in connection with the GFDL data set. They appreciate the assistance of H. A. Burgdorf and C. K. Chen in data processing and the technical assistance of L. K. Calvin, B. G. Miller and R. L. Rees.

The authors gratefully acknowledge the constructive comments by the reviewers of this paper and Dr. R. D. Rosen of Atmospheric and Environmental Research, Inc., in revising the original manuscript.

The research was supported jointly by the National Science Foundation, the National Oceanic and Atmospheric Administration and the National Aeronautics and Space Administration under GARP Grant NSF ATM-8108216.

REFERENCES

Baker, W. E., E. C. Kung and R. C. J. Somerville, 1977: Energetics diagnosis of the NCAR general circulation model. *Mon. Wea. Rev.*, **105,** 1384–1401.

——, —— and ——, 1978: An energetics analysis of forecast experiments with the NCAR general circulation model. *Mon. Wea. Rev.*, **106,** 311–323.

Bengtsson, L., M. Kanamitsu, P. Kållberg and S. Uppala, 1982: FGGE 4-dimensional data assimilation at ECMWF. *Bull. Amer. Meteor. Soc.*, **63,** 29–43.

Chen, T. G., and L. F. Bosart, 1977: Quasi-Lagrangian kinetic energy budgets of composite cyclone-anticyclone couplets. *J. Atmos. Sci.*, **34,** 452–470.

Fuelberg, H. E., and J. R. Scoggins, 1980: Kinetic energy budget during strong jet stream activity over the eastern United States. *Mon. Wea. Rev.*, **108,** 69–77.

Holopainen, E. O., and K. Eerola, 1979: A diagnostic study of the long-term balance of kinetic energy of atmospheric large-scale motion over the British Isles. *Quart. J. Roy. Meteor. Soc.*, **105,** 849–858.

Kung, E. C., 1967: Diurnal and long-term variation of the kinetic energy generation and dissipation for a five-year period. *Mon. Wea. Rev.*, **95,** 593–606.

——, 1969: Further study on the kinetic energy balance. *Mon. Wea. Rev.*, **97,** 573–581.

——, 1977: Large-scale energy transformations in the intense winter monsoon over the Kuroshio region. *J. Meteor. Soc. Japan,* **55,** 498–510.

——, and P. H. Chan, 1981: Energetics characteristics of the Asian winter monsoon in the source region. *Mon. Wea. Rev.*, **109,** 854–870.

Lorenz, E. N., 1955: Available potential energy and the maintenance of the general circulation. *Tellus,* **7,** 157–167.

Manabe, S., J. Smagorinsky, J. L. Holloway, Jr. and H. M. Stone, 1970: Simulated climatology of a general circulation model with a hydrologic cycle: III. Effects of increased horizontal computational resolution. *Mon. Wea. Rev.*, **98,** 175–212.

McPherson, R. D., K. H. Bergman, R. E. Kistler, G. E. Rasch and D. S. Gordon, 1979: The NMC operational global data assimilation system. *Mon. Wea. Rev.*, **107,** 1445–1461.

Miyakoda, K., J. Sheldon and J. Sirutis, 1982: Four-dimensional analysis experiment during the GATE period. Part II. *J. Atmos. Sci.*, **39,** 486–506.

Newell, R. E., D. G. Vincent, T. G. Dopplick, D. Ferruzza and J. W. Kidson, 1970: The energy balance of the global atmosphere. *Global Circulation of the Atmosphere,* G. S. Corby, Ed., Roy. Meteor. Soc., 42–90.

Oort, A. H., 1964: On estimates of the atmospheric energy cycle. *Mon. Wea. Rev.*, **92,** 483–493.

——, and J. P. Peixoto, 1974: The annual cycle of the energetics of the atmosphere on a planetary scale. *J. Geophys. Res.*, **79,** 2705–2719.

Saltzman, B., 1957: Equations governing the energetics of the larger scales of atmospheric turbulence in the domain of wavenumber. *J. Meteor.*, **14,** 513–523.

——, 1970: Large-scale atmospheric energetics in the wavenumber domain. *Rev. Geophys. Space Phys.*, **8,** 289–302.

——, and A. Fleisher, 1960: The mode of release of available potential energy in the atmosphere. *J. Geophys. Res.*, **65,** 1213–1222.

Smagorinsky, J., S. Manabe and J. L. Holloway, Jr., 1965: Numerical results from a nine-level general circulation model of the atmosphere. *Mon. Wea. Rev.*, **93,** 727–768.

Smith, P. J., and S. Adhikary, 1974: The dissipation of kinetic energy in large-scale atmospheric circulations. *Rev. Geophys. Space Phys.*, **12,** 281–284.

Williamson, D., and C. Temperton, 1981: Normal mode initialization for a multi-level grid-point model. Part II: Nonlinear aspects. *Mon. Wea. Rev.*, **109,** 744–757.

Wiin-Nielsen, A., 1968: On the intensity of the general circulation of the atmosphere. *Rev. Geophys.*, **6,** 559–579.